Stick-Slip and Slip-Slip Operation of Piezoelectric Inertia Drives – Part I: Ideal Excitation[☆]

Matthias Hunstig*, Tobias Hemsel*, Walter Sextro*

Mechatronics and Dynamics, University of Paderborn, Pohlweg 47 - 49, 33098 Paderborn, Germany

Abstract

Piezoelectric inertia motors, also known as "stick-slip drives", use the inertia of a body to drive it in small steps by means of a friction contact. While these steps are classically assumed to involve stiction and sliding, the motors can also operate in "slip-slip" mode without any phase of static friction. This contribution provides a systematic investigation and performance comparison of different stick-slip and slip-slip modes of operation. Different criteria for comparing the motional performance of inertia motors are defined: Steady state velocity, smoothness of motion, and start-up time. Using the example of a translational inertia motor excited by an ideal displacement signal, it is found that the maximum velocity reachable in stick-slip operation is limited principally, while continuous slip-slip operation allows very high velocities. For the investigated driving signals, the motor velocity is proportional to the square root of the actuator stroke. The motor performance with these ideal signals defines an upper boundary for the performance of real motors.

Keywords: inertia motor, stick-slip drive, mode of operation, performance indicator, velocity maximization, actuator stroke

1. Introduction

Piezoelectric inertia motors have originally been developed in the mid-1980s for fine positioning applications in the laboratory [1, 2, 3], but found application in several other fields in the last years, often in miniaturized consumer goods [4, 5, 6, 7, 8]. This was facilitated by the fact that inertia motors have a simple construction and are controlled by a single signal, which allows for low

*Corresponding author. Telephone: +49 5251 60 1813; fax: +49 5251 60 1803; e-mail: matthias.hunstig@upb.de

Email addresses: matthias.hunstig@upb.de (Matthias Hunstig), tobias.hemsel@upb.de (Tobias Hemsel), walter.sextro@upb.de (Walter Sextro)

Accepted manuscript, submitted to Sensors and Actuators A: Physical, 3 September 2012

production costs and simplifies miniaturization. Recent development trends are the simultaneous use of two eigenmodes of the stator component to produce high velocity inertia motors [9, 10, 11, 12], compact inertia motors that require only one drive signal to operate with two degrees of freedom [13, 8], and controlled force generation with inertia motors [14, 15].

Inertia motors use the inertia of a body to drive it by means of a friction contact in a series of small steps. Motors of this type are also known as "stick-slip drives" because these steps are classically regarded to be composed of a phase of static friction between the driving and the driven part and a phase where the two parts slide on each other. But inertia motors can successfully operate also without phases of static friction, which is known as the "slip-slip" mode.

This fact has been gaining wider recognition since only a few years. Some authors [16, 8, 11] have described inertia motors operating in both stick-slip and slip-slip mode, but the principal advantages, disadvantages und limitations of the two modes of operation are still unclear. This contribution aims to provide a systematic investigation of different modes of operation of inertia motors and of the maximum motor performance achievable in these modes under ideal conditions.

The model of a translational inertia motor excited by a displacement signal, which is the basis of this investigation, is introduced in section 2. Different values that describe the motional performance of an inertia motor are identified and clearly defined in section 3. In section 4, four different drive signals (stepping or continuous motion; stick-slip or slip-slip) that maximize the motor velocity are derived from the model, and the performance of the motor using these signals is determined. As they are derived assuming an ideal actuator with unlimited velocity and acceleration, these values define an upper boundary for the performance of real motors. The conclusions are presented in section 5. The performance of inertia motors driven with frequency-limited signals derived from the ideal signals presented in this contribution is left for future work.

2. Model and definitions

2.1. Motor

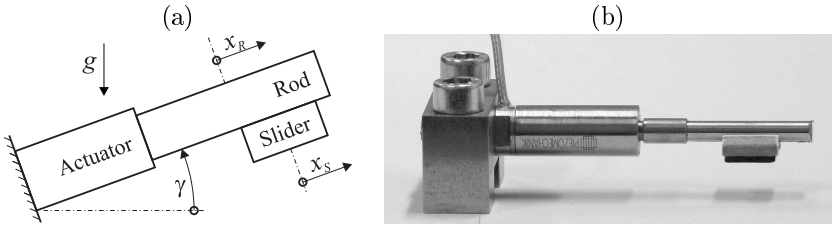

Figure 1: (a) Schematic view of a fixed-actuator type inertia motor and (b) photo of an example of such a motor

Figure 1(a) shows a schematic view of the investigated type of motor: A rigidly mounted – usually piezoelectric – actuator has a rod attached to its tip. A slider hangs below the driving rod. It is pressed against the rod by an additional contact force, usually resulting from elastic deformation or magnetic attraction. Figure 1(b) shows an example of such a motor constructed in the authors' lab: The pre-stressed piezoelectric multilayer actuator (PSt 150/5/20 from Piezomechanik GmbH) has a steel rod attached to its tip. According to the manufacturer and validated by experiments [17, 18], it has a stroke of 27 µm in quasistatic operation when driven with the maximum allowed voltage of -30 to +150 V. Experiments have shown that, depending on the mass of the rod, this stroke can be obtained at frequencies up to at least some kilohertz. For the following calculations, a maximum stroke of 25 µm was assumed in order to compensate for possible degradation of the actuator performance, and to allow a small safety margin from the maximum allowed voltage. The slider is made of aluminium with glued-on alumina (Al_2O_3) friction pads as the contact interface. It is pressed against the rod by the magnetic attraction force exerted by a magnet that is fixed at the opposite side of the slider. The attraction force and the coefficients of friction for this setup have been determined by the authors in unpublished experiments. Table 1 contains a list of all relevant parameters of the test motor and their values.

It should be emphasized that the following investigations and results are not only valid for this specific motor, but of general validity for this motor type – the motor parameters in table 1 and the gravity constant $g = 9.81\,\mathrm{m\,s^{-1}}$ have only been used to generate the diagrams presented in chapter 4.

Parameter	Symbol	Value
rod mass	m_R	2.6 g
slider mass	m_S	1.4 g
maximum rod displacement	$x_{R,\max}$	25 µm
additional contact force	F_M	1 N
coefficient of sliding (dynamic) friction	μ_d	0.16
coefficient of static friction (stiction)	μ_0	$1.1 \cdot \mu_d = 0.176$
angle of rod orientation	γ	0

Table 1: Parameters of a test motor, used to calculate the diagrams in chapter 4

2.2. Model

Figure 2 shows the model which is the basis of the following analysis. A slider of mass m_s hangs below the driving rod. $x_R(t)$ and $x_S(t)$ are the displacements of rod and slider, respectively. The contact force F_c between rod and slider results from the gravitational force F_g and an external force F_M, both assumed to act on the center of gravity C of the slider. The friction force $F_f(t)$ acts between rod and slider.

In this first part of the analysis, the usually piezoelectric actuator that moves the rod is not considered and the displacement $x_R(t)$ of the rod is regarded as

the system input which is limited by

$$0 \leq x_R(t) \leq x_{R,\max}. \tag{1}$$

Velocity $\dot{x}_R(t)$ and acceleration $\ddot{x}_R(t)$ of the rod are not limited. The following additional assumptions and simplifications are made:

- Rod and slider are regarded as rigid bodies. This assumption is valid as long as the highest excitation frequency is much smaller than the first eigenfrequency of rod or slider, whichever is lower.
- The rod is excited purely axially, there is no lateral movement.
- Rotational effects of all forces are neglected.

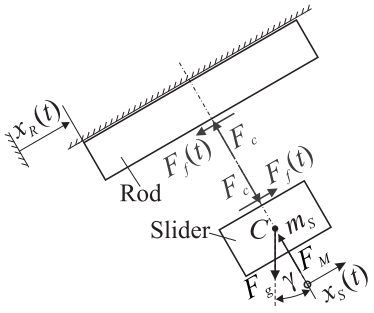

Figure 2: Rigid body model of a simple translational inertia motor

The equation of motion of the slider is

$$m_S \ddot{x}_S(t) = -F_g \sin\gamma + F_f(t), \tag{2}$$

with $F_g = m_S g$.

In this analysis, the friction force $F_f(t)$ is modelled using a Coulomb friction model with constant coefficients of static and dynamic friction μ_0 and μ_d. It can therefore be described by

$$F_f(t) = \begin{cases} m_S \ddot{x}_R(t) + F_g \sin\gamma & \text{if } \dot{x}_R(t) = \dot{x}_S(t) \\ & \wedge\ |m_S \ddot{x}_R(t) + F_g \sin\gamma| \leq F_{f,0,\max} \\ \mu_d F_c \operatorname{sgn}\left(\dot{x}_R(t) - \dot{x}_S(t)\right) & \text{if } \dot{x}_R(t) \neq \dot{x}_S(t) \\ & \vee\ |m_S \ddot{x}_R(t) + F_g \sin\gamma| > F_{f,0,\max} \end{cases} \tag{3}$$

with the maximum transmissible force in stiction $F_{f,0,\max} = \mu_0 F_c$ and the normal contact force $F_c = -F_g \cos\gamma + F_M$.

2.3. Definitions

The break-away acceleration $a_0(t)$ of the rod, above which the slider starts to slide, is found from $F_{f,0,\max}$ and the equation of motion (2) as

$$a_0(t) = -g\sin(\gamma) + \operatorname{sgn}(\ddot{x}_R(t))\frac{\mu_0 F_c}{m_S} \tag{4}$$

The acceleration of the slider during sliding is determined from (2) and (3) as:

$$a_d(t) = -g\sin(\gamma) + \operatorname{sgn}(\dot{x}_R(t) - \dot{x}_S(t))\frac{\mu_d F_c}{m_S} \tag{5}$$

$a_0(t)$ and $a_d(t)$ are functions of time but if g, γ, μ_0, μ_d, and F_M are constant as they are in many applications, the two accelerations can only take two different values each. These values can be regarded as characteristic accelerations of the motor system. To simplify the following calculations, these four accelerations are given individual symbols:

$$a_0^+ = a_0(\ddot{x}_R > 0) = -g\sin(\gamma) + \frac{\mu_0 F_c}{m_S} \tag{6}$$

$$a_0^- = a_0(\ddot{x}_R < 0) = -g\sin(\gamma) - \frac{\mu_0 F_c}{m_S} \tag{7}$$

$$a_d^+ = a_d(\dot{x}_R - \dot{x}_S > 0) = -g\sin(\gamma) + \frac{\mu_d F_c}{m_S} \tag{8}$$

$$a_d^- = a_d(\dot{x}_R - \dot{x}_S < 0) = -g\sin(\gamma) - \frac{\mu_d F_c}{m_S} \tag{9}$$

It can be shown that in every motor capable of bidirectional movement, the characteristic accelerations have a fixed sign corresponding to their superscript:

$$a_0^+ > 0 \qquad a_0^- < 0 \qquad a_d^+ > 0 \qquad a_d^- < 0$$

In the following chapters only operation with slider movement in positive direction of x_S is treated. Movement in negative direction of x_S can be treated analogously.

3. Motional performance indicators

3.1. Steady state velocity

In an inertia motor, the slider does not have a constant velocity by principle. Figure 3 shows a typical oscillation of the slider velocity in steady state around the steady state velocity $\bar{v}_\infty$. Similar velocity profiles have been found in experiments by Okamoto and Yoshida [16] and – shown in figure 4 – by the authors with the motor described in section 2.1.

In many cases, the mean velocity of an inertia motor slider increases asymptotically period by period. Figure 5 shows such a typical velocity increase. Such transient behaviour has been observed in experiments by the authors and others

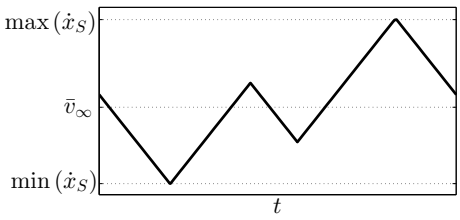

Figure 3: Typical idealised slider velocity $\dot{x}_S(t)$ in steady state

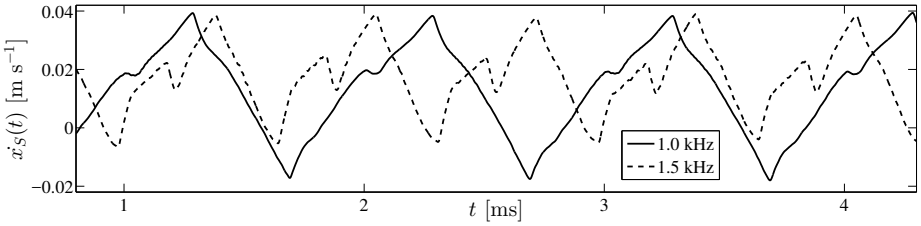

Figure 4: Measured slider velocity slider in the test motor described in section 2.1 in steady state at different excitation frequencies

[16, 19, 11]. In the following, $\bar{v}_p$ is the mean slider velocity in the p-th period and the steady state velocity $\bar{v}_\infty$ is defined as

$$\bar{v}_\infty = \lim_{p \to \infty} \bar{v}_p. \tag{10}$$

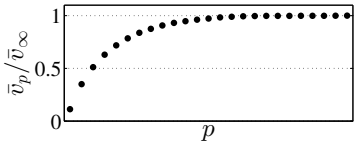

Figure 5: Typical velocity increase of an inertia motor at start-up, shown over the number of periods p

3.2. Start-up time

Unless in some rare ideal cases where $\bar{v}_\infty$ is reached in a finite number of periods, the start-up time of an inertia motor is not clearly defined. It therefore makes sense to define a threshold percentage q of $\bar{v}_\infty$. In the following, p_q is the first period during which $\bar{v}_{p_q} \geq q \cdot \bar{v}_\infty$ and the start-up time is $T \cdot p_q$, where T is the period of the excitation signal. As $\bar{v}_p$ is defined over complete periods only, the start-up time following this definition is always a multiple of T. For example, $T \cdot p_{0.99}$ is the time after which $\bar{v}_p \geq 0.99\,\bar{v}_\infty$. In the following, $T \cdot p_{0.99}$ is called the start-up time.

3.3. Smoothness indicator

In any application, a smooth slider motion is desired. In the following, the magnitude of the inverse of the relative spread between minimum und maximum slider velocity is used as the indicator ς_p for the smoothness of the slider motion in period p:

$$\varsigma_p = \frac{|\bar{v}_p|}{\max_p\left(\dot{x}_S(t)\right) - \min_p\left(\dot{x}_S(t)\right)} \tag{11}$$

The smoother the motion of the slider is, the higher becomes ς_p. In the following, the smoothness indicator for steady state, $\varsigma_\infty = \lim_{p\to\infty} \varsigma_p$, is compared.

4. Ideal excitation signals for maximum velocity

In many applications of inertia motors, especially in consumer applications, high velocity is a primary design goal. In this chapter, drive signals $x_R(t)$ that maximize the steady state velocity of the slider under different requirements are described and the motional performance indicators are determined for these modes. The differences between the four presented modes are whether the slider is accelerated by stiction or sliding friction and whether it is making discrete steps or continuously moving.

For each mode, typical plots of displacement, velocity, and acceleration of rod and slider over time are presented. These plots were calculated using the analytical equations derived in the respective sections with the parameters given in table 1 and the constants defined in section 2.3. Positive and negative infinite velocities and accelerations are indicated in the plots by arrows pointing up or down, respectively.

4.1. Discrete "stepping" stick-slip operation

4.1.1. Movement cycle

In discrete or stepping stick-slip mode, the slider is accelerated by stiction and moves in a series of discrete steps between which the whole motor is at rest. Fig. 6 shows displacement, velocity, and acceleration of rod and slider in this mode of operation. The movement cycle for maximum velocity in this mode consists of three phases which are continously repeated:

1. Acceleration phase (length Δt_1): The rod accelerates with $a_R = \kappa a_0^+$ until it reaches its maximum position $x_{R,\max}$, with $\kappa \leq 1$ so that the slider sticks to the rod and thus makes the same movement.
2. Pull-back (infinitely short): The rod returns to $x_R(t) = 0$. Due to the assumption of unlimited rod velocity and acceleration, this phase is infinitely short. The (infinite) rod acceleration is larger than a_0^+, thus the slider starts to slide.
3. Deceleration phase (length Δt_2): The rod is at rest, the slider is continuously decelerated by sliding friction until it also comes to rest.

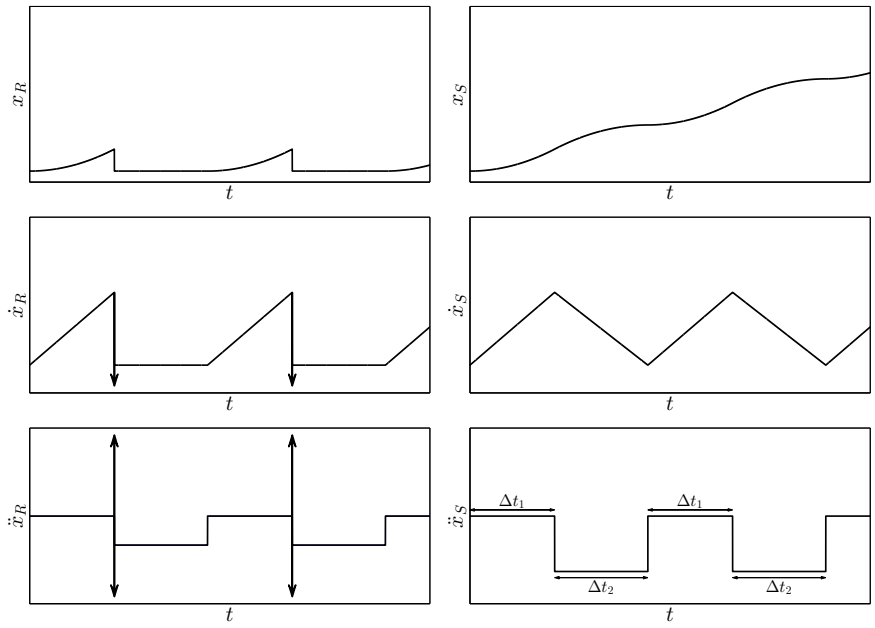

Figure 6: Displacement (x), velocity ($\dot{x}$), and acceleration ($\ddot{x}$) of rod (index $_R$) and slider (index $_S$) in discrete stick-slip operation. All scales of the same type (time, displacement, velocity, acceleration) are equal.

4.1.2. Analysis

Acceleration phase. During the first acceleration phase after a start from rest, the movement of rod and slider is described by:

$$\begin{aligned} \ddot{x}_R(t) = \ddot{x}_S(t) =& a_R \\ \dot{x}_R(t) = \dot{x}_S(t) =& a_R t \\ x_R(t) = x_S(t) =& \frac{a_R}{2} t^2 \end{aligned} \tag{12}$$

The acceleration phase ends when the rod has reached its maximum deflection, i. e. when $x_R(t) = x_{R,\max}$. The length Δt_1 of this phase is determined by

$$\Delta t_1 = \sqrt{\frac{2x_{R,\max}}{a_R}} \tag{13}$$

and at the end of this phase rod and slider have the same velocity v_1:

$$v_1 = \sqrt{2x_m a_R} \tag{14}$$

Pull-back phase. During this phase, the acceleration of the rod becomes infinitely large first in in negative and then in positive direction. The velocity of the rod becomes infinintely large in negative direction. The position of the rod

jumps from $x_R(\Delta t_1) = x_{R,\max}$ to $x_R(\Delta t_1) = 0$. As this phase is infinitely short, the slider does not move in this phase.

Deceleration phase. During the deceleration phase, the movement of rod and slider is described by:

$$\ddot{x}_R(t) = 0 \qquad \dot{x}_R(t) = 0 \qquad x_R(t) = 0 \tag{15}$$

$$\begin{aligned} \ddot{x}_S(t) &= a_d^- \\ \dot{x}_S(t) &= v_1 + a_d^-(t - \Delta t_1) \\ x_S(t) &= x_{R,\max} + v_1(t - \Delta t_1) + \frac{a_d^-}{2}(t - \Delta t_1)^2 \end{aligned} \tag{16}$$

The deceleration phase ends when the slider velocity reaches zero, i. e. when $\dot{x}_S(\Delta t_1 + \Delta t_2) = 0$. From this condition follows the length Δt_2 of this phase as

$$\Delta t_2 = -\frac{v_1}{a_d^-} = -\frac{\sqrt{2 x_{R,\max} a_R}}{a_d^-}. \tag{17}$$

4.1.3. Motional performance

In modes of operation with discrete steps, the step size and the mean velocity remain constant in each period. At the end of the deceleration phase the slider has completed its step, thus the step size is

$$\bar{x}_\infty = x_S(\Delta t_1 + \Delta t_2) = \left(1 - \frac{a_R}{a_d^-}\right) x_{R,\max}. \tag{18}$$

The period is

$$T = \Delta t_1 + \Delta t_2 = \sqrt{2 x_{R,\max}} \left(\frac{1}{\sqrt{a_R}} - \frac{\sqrt{a_R}}{a_d^-}\right). \tag{19}$$

The steady state velocity is $\bar{v}_\infty = \bar{x}_\infty / T$. Because of the purely linear change of the slider velocity – cp. figure 6 – it can also be calculated as $\bar{v}_\infty = v_1/2$. Both formulas lead to:

$$\bar{v}_\infty = \sqrt{\frac{x_{R,\max} a_R}{2}} \tag{20}$$

The steady state velocity is reached already in the first period, which means that $p_{0.99} = 1$ and therefore the start-up time is

$$T \cdot p_{0.99} = T = \sqrt{2 x_{R,\max}} \left(\frac{1}{\sqrt{a_R}} - \frac{\sqrt{a_R}}{a_d^-}\right). \tag{21}$$

The smoothness indicator becomes:

$$\varsigma_\infty = \frac{|\bar{v}_\infty|}{v_{\max,\infty} - v_{\min,\infty}} = \frac{\bar{v}_\infty}{v_1 - 0} = \frac{1}{2}. \tag{22}$$

4.2. Continuous stick-slip operation

4.2.1. Movement cycle

In this mode of operation the deceleration phase is minimized. The slider is continuously in motion in this mode which is thus called the continuous mode of operation. Fig. 7 shows displacement, velocity, and acceleration of rod and slider in this mode of operation. The movement cycle for maximum velocity consists of four phases, phases 2 to 4 are continuously repeated:

1. First acceleration phase (length Δt_1): The rod accelerates with $a_R = \kappa a_0^+$ until it reaches its maximum position $x_{R,\max}$. As $\kappa \leq 1$ in this stick-slip mode, the slider sticks to the rod and thus makes the same movement.
2. Pull-back (infinitely short): The rod returns to $x_R(t) = 0$. Due to the assumption of unlimited rod velocity and acceleration, this phase is infinitely short. The (infinite) rod acceleration is larger than a_0^+, the slider begins to slide on the rod.
3. Decelaration phase (length Δt_2): The rod again accelerates with a_R. Because the slider velocity is still higher than the rod velocity, the slider is continuously decelerated by sliding friction.
4. Acceleration phase (length $\Delta t_1 - \Delta t_2$): When (increasing) rod velocity and the (decreasing) slider velocity are equal, a new phase of stiction begins during which the slider moves with the rod and is thus accelerated with a_R.

4.2.2. Analysis

First acceleration phase. The first acceleration phase in continuous stick-slip operation is identical to the acceleration phase in discrete operation described in section 4.1.2.

Pull-back phase. This phase is identical to the pull-back phase in discrete operation described in section 4.1.2.

Deceleration phase. During the deceleration phase, the slider moves like in the discrete mode (equations (16)). But the rod is accelerated again with a_R directly after it has returned to its starting position. Its movement is described by

$$\begin{aligned} \ddot{x}_R(t) =& a_R \\ \dot{x}_R(t) =& a_R(t - \Delta t_1) \\ x_R(t) =& \frac{a_R}{2}(t - \Delta t_1)^2 \end{aligned} \tag{23}$$

The deceleration phase ends when the (decelerating) slider and the (accelerating) rod reach the same velocity. From this condition the length Δt_2 of this phase is found by equating $\dot{x}_S(\Delta t_1 + \Delta t_2) = \dot{x}_R(\Delta t_1 + \Delta t_2)$ (equations (16) and (23)) as

$$\Delta t_2 = \frac{v_1}{a_R - a_d^-} \tag{24}$$

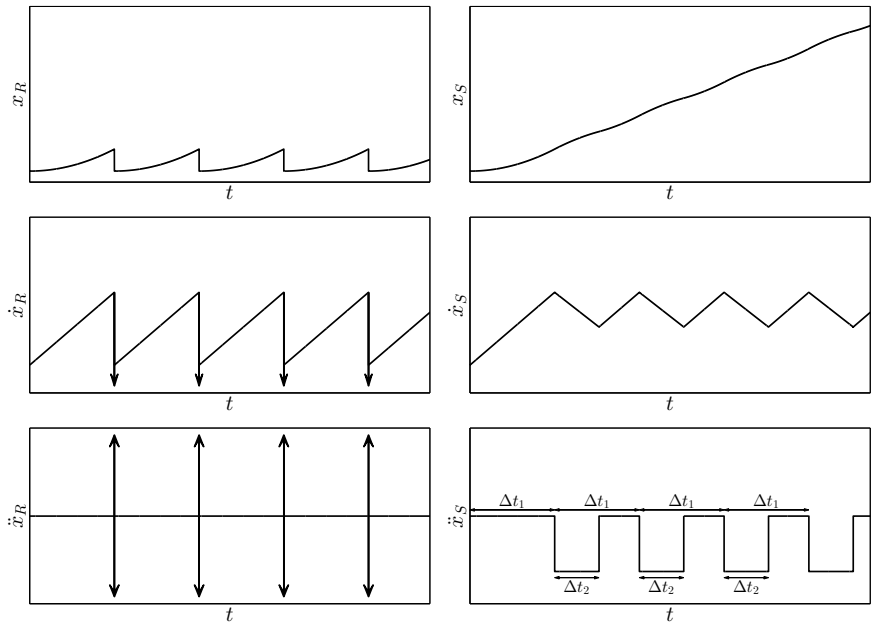

Figure 7: Displacement (x), velocity ($\dot{x}$), and acceleration ($\ddot{x}$) of rod (index $_R$) and slider (index $_S$) in continuous stick-slip operation. All scales of the same type (time, displacement, velocity, acceleration) are equal and as in figure 6.

Substituting (24) into (16) or (23) gives the (equal) velocities v_2 of rod and slider at the end of the deceleration phase:

$$v_2 = \dot{x}_S(\Delta t_1 + \Delta t_2) = \dot{x}_R(\Delta t_1 + \Delta t_2) = v_1 \frac{a_R}{a_R - a_d^-}. \tag{25}$$

Acceleration Phase. Once slider and rod reach the same velocity, the slider again sticks to the rod. Because the rod is not at $x_R(t) > 0$ at the beginning of this phase, it is shorter than the first acceleration phase. Because of the purely linear velocity change, its length can be calculated as

$$\Delta t_1 - \Delta t_2 = \frac{v_1 - v_2}{a_R}. \tag{26}$$

This phase ends when the rod again reaches its maximum position at $t = 2\,\Delta t_1$. The velocity of rod and slider at the end of this phase is

$$\dot{x}_R(2\,\Delta t_1) = \dot{x}_S(2\,\cdot\Delta t_1) = a_R \cdot \Delta t_1. \tag{27}$$

Full Cycle. After the first acceleration phase the slider moves in a steady state cycle of acceleration and deceleration. This cycle has the period

$$T = \Delta t_1 = \sqrt{\frac{2x_{R,\max}}{a_R}}. \tag{28}$$

4.2.3. Motional Performance

The steady state velocity of the slider is calculated as:

$$\bar{v}_\infty = \frac{v_1 + v_2}{2} = \sqrt{\frac{x_{R,\max} a_R}{2}} \left(1 + \frac{a_R}{a_R - a_d^-}\right) \tag{29}$$

The steady state step size follows as:

$$\bar{x}_\infty = \bar{v}_\infty \cdot \Delta t_1 = x_{R,\max} \left(1 + \frac{a_R}{a_R - a_d^-}\right) \tag{30}$$

The steady state velocity is reached in the second period. Unless $\mu_d \gg \mu_0$, which cannot be the case in real systems, the mean velocity in the first period is significantly below the steady state velocity. So $p_{0.99} = 2$ is true for all relevant systems and therefore the start-up time is

$$T \cdot p_{0.99} = 2\sqrt{\frac{2x_{R,\max}}{a_R}}. \tag{31}$$

Applying (14), (25), and (29) to (11), the smoothness indicator becomes

$$\varsigma_\infty = \frac{|\bar{v}_\infty|}{v_{\max,\infty} - v_{\max,\infty}} = \frac{\bar{v}_\infty}{v_1 - v_2} = \frac{1}{2} - \frac{a_R}{a_d^-}. \tag{32}$$

4.3. Accelerating stick-slip operation

The length of the deceleration phase in continuous stick-slip operation could be reduced if the rod acceleration was higher than a_0^+ in this phase. In this mode of operation, the mean slider velocity would rise from period to period. It is therefore called the accelerating mode of operation. Assuming unlimited rod acceleration, this phase could become infinitely short. The slider velocity would then be described by $\dot{x}_S(t) = a_R \cdot t$.

For a correct determination of the driving signal for this mode it would be necessary to exactly know the current slider velocity, which required a sensor. Also, the driving signal is not periodic in this mode of operation and has to be recalculated every period, which requires a powerful signal generator. For these reasons, practical realization of this mode is very difficult and costly. It is therefore not discussed any further in this contribution. Short discussions of this mode and model calculations in which it is applied using excitation signals with limited acceleration can be found in [20] and [21].

4.4. Discrete slip-slip operation

In the stick-slip modes of operation discussed above, the slider is accelerated with $a_R = \kappa a_0^+$, with $\kappa \leq 1$. The maximum acceleration possible using stiction is achieved with $\kappa = 1$. If the rod acceleration in the acceleration phase is increased above a_0^+ (i. e. if $\kappa > 1$), there is no more stiction in this phase and the slider is accelerated by sliding friction. The motor is than said to operate in

slip-slip mode. Both a discrete and a continuous slip-slip mode can be realized analogously to the stick-slip modes.

These modes are analysed in this and the following section. It should be noted that the discrete steps in discrete slip-slip mode require rod and slider to be at rest at least for an infinitely short time at the end of every period. Though labelled "slip-slip", this mode is therefore not strictly "sliding only".

4.4.1. Movement cycle

The movement cycle of rod and slider in this mode only differs from the cycle of the discrete stick-slip mode described in section 4.1.1 by the acceleration magnitudes in the acceleration phase. Figure 8 shows displacement, velocity, and acceleration of rod and slider in this mode of operation.

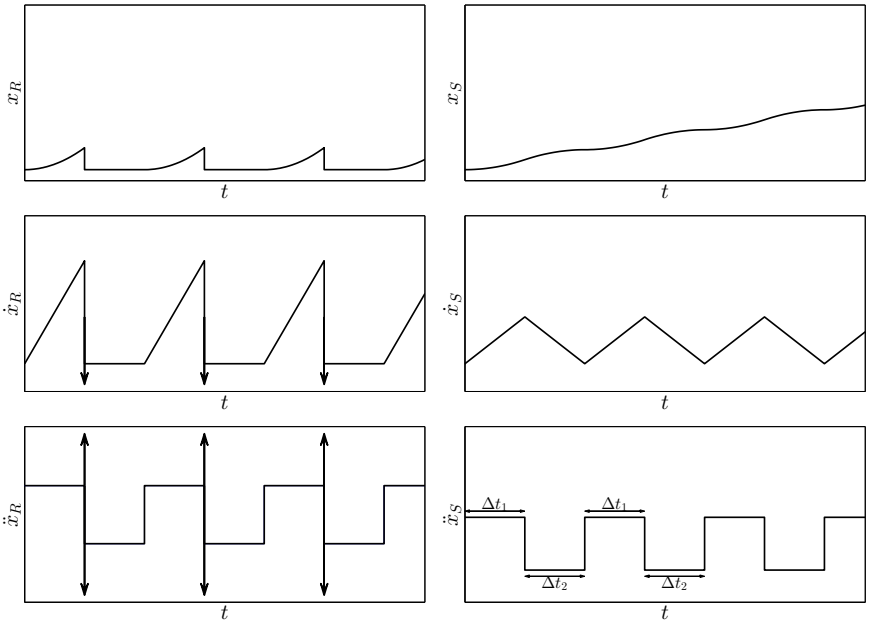

Figure 8: Displacement (x), velocity ($\dot{x}$), and acceleration ($\ddot{x}$) of rod (index $_R$) and slider (index $_S$) in discrete slip-slip operation with $\kappa = a_R/a_0^+ = 2$. All scales of the same type (time, displacement, velocity, acceleration) are equal and as in figure 6.

4.4.2. Analysis

Acceleration phase. During the acceleration phase, the movement of rod and slider is described by:

$$\begin{aligned} \ddot{x}_R(t) &= a_R \\ \dot{x}_R(t) &= a_R t \\ x_R(t) &= \frac{a_R}{2} t^2 \end{aligned} \tag{33}$$

$$\begin{aligned}\ddot{x}_S(t) &= a_d^+ \\ \dot{x}_S(t) &= a_d^+ t \\ x_S(t) &= \frac{a_d^+}{2} t^2\end{aligned} \tag{34}$$

The acceleration phase ends when the rod has reached its maximum deflection, i. e. when $x_R(t) = x_{R,\max}$. As in the other modes of operation, the length Δt_1 of this phase is determined by

$$\Delta t_1 = \sqrt{\frac{2x_{R,\max}}{a_R}}. \tag{35}$$

At the end of this phase the slider has the velocity

$$v_1 = a_d^+ \sqrt{\frac{2x_{R,\max}}{a_R}} \tag{36}$$

and is at the position

$$x_1 = \frac{v_1 \Delta t_1}{2} = x_{R,\max} \frac{a_d^+}{a_R}. \tag{37}$$

Pull-back phase. During this phase, the acceleration of the rod becomes infinitely large first in negative and then in positive direction. The velocity of the rod becomes infinintely large in negative direction. The position of the rod jumps from $x_R(\Delta t_1) = x_{R,\max}$ to $x_R(\Delta t_1) = 0$. The slider does not move during this infinitely short phase.

Deceleration phase. During the deceleration phase, the rod is at rest as in the discrete stick-slip mode of operation:

$$\ddot{x}_R(t) = 0 \qquad \dot{x}_R(t) = 0 \qquad x_R(t) = 0 \tag{38}$$

The slider movement in this phase is described by:

$$\begin{aligned}\ddot{x}_S(t) &= a_d^- \\ \dot{x}_S(t) &= v_1 + a_d^- (t - \Delta t_1) \\ x_S(t) &= x_1 + v_1 (t - \Delta t_1) + \frac{a_d^-}{2} (t - \Delta t_1)^2\end{aligned} \tag{39}$$

The deceleration phase ends when the slider velocity reaches zero, i. e. when $\dot{x}_S(t) = 0$. From this condition follows the length Δt_2 of this phase:

$$\Delta t_2 = -\frac{v_1}{a_d^-} = -\frac{a_d^+}{a_d^-} \sqrt{\frac{2x_{R,\max}}{a_R}} \tag{40}$$

4.4.3. Motional performance

In modes of operation with discrete steps, the step size and the mean velocity are the same in each period. At the end of the deceleration phase the slider has completed its step of

$$\bar{x}_\infty = x_S(\Delta t_1 + \Delta t_2) = \frac{a_d^+}{a_R}\left(1 - \frac{a_d^+}{a_d^-}\right) x_{R,\max} \tag{41}$$

in a period of

$$T = \Delta t_1 + \Delta t_2 = \left(1 - \frac{a_d^+}{a_d^-}\right)\sqrt{\frac{2x_{R,\max}}{a_R}}. \tag{42}$$

Due to the purely linear change of the slider velocity – cp. figure 8 – the mean velocity can be calculated either as $\bar{v}_\infty = \bar{x}_\infty/T$ or as $\bar{v}_\infty = v_1/2$. Both formulas lead to:

$$\bar{v}_\infty = a_d^+\sqrt{\frac{x_{R,\max}}{2a_R}} \tag{43}$$

As in the discrete stick-slip mode of operation, the steady state velocity is reached already in the first period, which means that $p_{0.99} = 1$ and therefore the start-up time is

$$T \cdot p_{0.99} = T = \left(1 - \frac{a_d^+}{a_d^-}\right)\sqrt{\frac{2x_{R,\max}}{a_R}}. \tag{44}$$

Following (11), the smoothness indicator becomes:

$$\varsigma_\infty = \frac{|\bar{v}_\infty|}{v_{\max,\infty} - v_{\min,\infty}} = \frac{\bar{v}_\infty}{v_1 - 0} = \frac{1}{2} \tag{45}$$

4.5. Continuous slip-slip operation

4.5.1. Movement cycle

As described above, a continuous slip-slip mode can be realized analogously to the continous stick-slip mode described in section 4.2, with the difference that $\kappa > 1$ so that the slider is accelerated by sliding friction instead of stiction.

Other than in the other modes with periodic drive signals, in continuous slip-slip mode the mean velocity of the slider continuously increases in every period asymptotically towards a saturation value. Figure 9 shows displacement, velocity, and acceleration of rod and slider in this mode of operation.

4.5.2. Analysis

The first period after start from rest ($p = 1$) consists only of one acceleration phase of length Δt_1, the following periods ($p \geq 2$) consist of a deceleration phase of length $\Delta t_{2,p}$ and an acceleration phase of length $\Delta t_1 - \Delta t_{2,p}$.

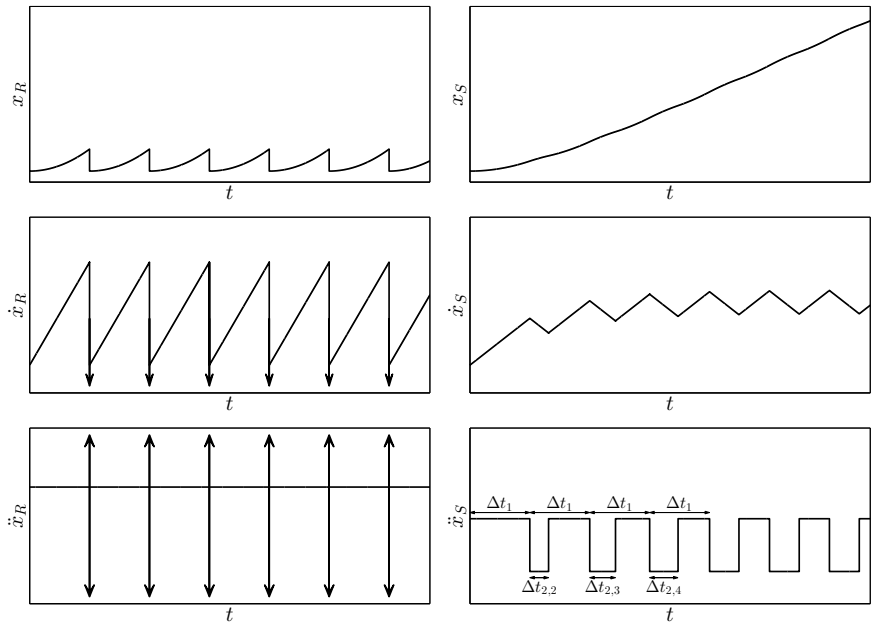

Figure 9: Displacement (x), velocity ($\dot{x}$), and acceleration ($\ddot{x}$) of rod (index $_R$) and slider (index $_S$) in continuous slip-slip operation with $\kappa = a/a_0^+ = 2$. All scales of the same type (time, displacement, velocity, acceleration) are equal and as in figure 6.

First acceleration phase. The first phase of acceleration from rest ($p = 1$) equals the acceleration phase of the discrete slip-slip mode described in section 4.4.2. This phase, and with it the first period, defining the cycle time, ends at

$$T = \Delta t_1 = \sqrt{\frac{2x_{R,\max}}{a_R}} \tag{46}$$

and at this time the slider has the velocity

$$\dot{x}_S(\Delta t_1) = a_d^+ \sqrt{\frac{2x_{R,\max}}{a_R}}. \tag{47}$$

and is at the position

$$x_S(\Delta t_1) = \frac{\dot{x}_S(\Delta t_1)\Delta t_1}{2} = x_{R,\max}\frac{a_d^+}{a_R}. \tag{48}$$

Pull-back phase. The pull-back phase of the continuous mode equals the pull-back phase of the discrete slip-slip mode described in section 4.4.2.

Deceleration phase. During the deceleration phases ($p \geq 2$), the slider movement is described by

$$\begin{aligned}
\ddot{x}_S(t) &= a_d^- \\
\dot{x}_S(t) &= \dot{x}_S((p-1)\Delta t_1) + a_d^-(t-(p-1)\Delta t_1) \\
x_S(t) &= x_S((p-1)\Delta t_1) + v_1(t-(p-1)\Delta t_1) + \frac{a_d^-}{2}(t-(p-1)\Delta t_1)^2
\end{aligned} \tag{49}$$

while the rod is accelerated again with a_R directly after it has returned to its starting position. Its movement is described by:

$$\begin{aligned}
\ddot{x}_R(t) &= a_R \\
\dot{x}_R(t) &= a_R(t-(p-1)\Delta t_1) \\
x_R(t) &= \frac{a_R}{2}(t-(p-1)\Delta t_1)^2
\end{aligned} \tag{50}$$

The deceleration phase ends when the (decelerating) slider and the (accelerating) rod reach the same velocity. From this condition the length of the first deceleration phase $\Delta t_{2,2}$ is found by equating $\dot{x}_S(\Delta t_1 + \Delta t_{2,2}) = \dot{x}_R(\Delta t_1 + \Delta t_{2,2})$ (equations (49) and (50)) as

$$\Delta t_{2,2} = \frac{v_1}{a_R - a_d^-} = \frac{a_d^+}{a_R - a_d^-}\sqrt{\frac{2x_{R,\max}}{a_R}}. \tag{51}$$

Substituting (51) into (49) or (50) gives the velocity $v_{S,\min,2}$ of rod and slider at the end of the first deceleration phase:

$$\begin{aligned}
v_{S,\min,2} &= \dot{x}_S(\Delta t_1 + \Delta t_{2,2}) = \dot{x}_R(\Delta t_1 + \Delta t_{2,2}) \\
&= v_1\frac{a_R}{a_R - a_d^-} = \frac{a_d^+}{a_R - a_d^-}\sqrt{2x_{R,\max}a_R}.
\end{aligned} \tag{52}$$

Second acceleration phase. In this phase, the slider is again accelerated through sliding friction. Its motion is described by:

$$\begin{aligned}
\ddot{x}_S(t) &= a_d^+ \\
\dot{x}_S(t) &= v_{S,\min,2} + a_d^+(t-\Delta t_1 - \Delta t_{2,2}) \\
x_S(t) &= x_S(\Delta t_1 + \Delta t_{2,2}) + v_{2,1}(t-\Delta t_1 - \Delta t_{2,2}) + \frac{a_d^+}{2}(t-\Delta t_1 - \Delta t_{2,2})^2
\end{aligned} \tag{53}$$

This phase ends when the driving rod again reaches its maximum deflection $x_{R,\max}$ at $2\,\Delta t_1$.

At the end of the second acceleration phase, slider velocity and position are described by:

$$\dot{x}_S(2\,\Delta t_1) = v_{S,\min,2} + a_d^+(\Delta t_1 - \Delta t_{2,2}) \tag{54}$$

Comparing (47) and (54) shows that the slider movement in one cycle is different from the slider movement in the previous cycle: $\dot{x}_S(2\,\Delta t_1) \neq \dot{x}_S(\Delta t_1)$.

The minimum and maximum slider velocities reached in period p at $t = (p-1)\Delta t_1 + \Delta t_{2,p}$ and $t = p \cdot \Delta t_1$ are described by the following sequences (with $\Delta t_{2,1} = 0$ because there is no deceleration phase in the first period):

$$\begin{aligned} v_{S,\min,1} &= 0 \\ v_{S,\min,p} &= \dot{x}_S((p-1)\Delta t_1 + \Delta t_{2,p}) \\ &= v_{S,\max,p-1} + a_d^- \cdot \Delta t_{2,p} \qquad \text{for } p \in \mathbb{N}^+ \backslash \{1\} \qquad (55) \\ v_{S,\max,p} &= \dot{x}_S(p \cdot \Delta t_1) \\ &= v_{S,\min,p} + a_d^+(p \cdot \Delta t_1 - \Delta t_{2,p}) \qquad \text{for } p \in \mathbb{N}^+ \qquad (56) \end{aligned}$$

These sequences converge for $p \to \infty$ and so do the other characteristic times, velocities and displacements of the drive cycle. For steady state operation, different characteristic values can be described by relatively simply expressions.

Steady state operation. In steady state operation,

$$\lim_{p\to\infty} \frac{(\Delta t_1 - \Delta t_{2,p})}{\Delta t_{2,p}} = -\frac{a_d^-}{a_d^+}$$

and the velocity oscillates linearly between $v_{S,\max,\infty} = \dot{x}_S\left(p \cdot \Delta t_1\right)$ and $v_{S,\min,\infty} = \dot{x}_S\left((p-1) \cdot \Delta t_1 + \Delta t_{2,\infty}\right)$. The mean velocity is determined as

$$\bar{v}_\infty = \frac{v_{S,\max,\infty} + v_{S,\min,\infty}}{2} = \frac{a_d^+\left(a_d^- - 2a_R\right)}{a_d^- - a_d^+}\sqrt{\frac{x_{R,\max}}{2a_R}} \qquad (57)$$

and the slider motion per period ("step length") follows as

$$\bar{x}_\infty = \bar{v}_\infty T = x_{R,\max}\frac{a_d^+\left(a_d^- - 2a_R\right)}{\left(a_d^- - a_d^+\right)a_R}. \qquad (58)$$

4.5.3. Motional performance

The smoothness indicator becomes:

$$\varsigma_\infty = \frac{|\bar{v}_\infty|}{v_{S,\max,\infty} - v_{S,\min,\infty}} = \frac{1}{2} - \frac{a_R}{a_d^-} \qquad (59)$$

There is no closed solution for the start-up time in this mode of operation. But p_q can be determined from the sequences (55) and (56) by finding the minimum p which satisfies

$$\frac{v_{S,\max,p} + v_{S,\min,p}}{2} \geq q \cdot \bar{v}_\infty \qquad (60)$$

	discrete	continuous
	stick-slip	
T	$\sqrt{2x_{R,\max}}\left(\frac{1}{\sqrt{a_R}}-\frac{\sqrt{a_R}}{a_d^-}\right)$ (19)	$\sqrt{\frac{2x_{R,\max}}{a_R}}$ (28)
$\bar{x}_\infty$	$x_{R,\max}\left(1-\frac{a_R}{a_d^-}\right)$ (18)	$x_{R,\max}\left(1+\frac{a_R}{a_R-a_d^-}\right)$ (30)
$T\cdot p_{0.99}$	$\sqrt{2x_{R,\max}}\left(\frac{1}{\sqrt{a_R}}-\frac{\sqrt{a_R}}{a_d^-}\right)$ (21)	$2\sqrt{\frac{2x_{R,\max}}{a_R}}$ (31)
$\bar{v}_\infty$	$\sqrt{\frac{x_{R,\max}a_R}{2}}$ (20)	$\sqrt{\frac{x_{R,\max}a_R}{2}}\left(1+\frac{a_R}{a_R-a_d^-}\right)$ (29)
ς_∞	$\frac{1}{2}$ (22)	$\frac{1}{2}-\frac{a_R}{a_d^-}$ (32)
	slip-slip	
T	$\left(1-\frac{a_d^+}{a_d^-}\right)\sqrt{\frac{2x_{R,\max}}{a_R}}$ (42)	$\sqrt{\frac{2x_{R,\max}}{a_R}}$ (46)
$\bar{x}_\infty$	$x_{R,\max}\frac{a_d^+}{a_R}\left(1-\frac{a_d^+}{a_d^-}\right)$ (41)	$x_{R,\max}\frac{a_d^+\left(a_d^- -2a_R\right)}{\left(a_d^- -a_d^+\right)a_R}$ (58)
$T\cdot p_{0.99}$	$\left(1-\frac{a_d^+}{a_d^-}\right)\sqrt{\frac{2x_{R,\max}}{a_R}}$ (44)	no closed solution (see 4.5.3)
$\bar{v}_\infty$	$a_d^+\sqrt{\frac{x_{R,\max}}{2a_R}}$ (43)	$\frac{a_d^+\left(a_d^- -2a_R\right)}{a_d^- -a_d^+}\sqrt{\frac{x_{R,\max}}{2a_R}}$ (57)
ς_∞	$\frac{1}{2}$ (45)	$\frac{1}{2}-\frac{a_R}{a_d^-}$ (59)

Table 2: Formulas for different performance indicators in the four ideal modes of operation

4.6. Performance comparison

For a direct comparison of the different modes of operation described in this chapter, table 2 summarizes the formulas for period T, steady state step size $\bar{x}_\infty$, start-up time $T\cdot p_{0.99}$, steady state velocity $\bar{v}_\infty$, and steady state smoothness ς_∞. As they are derived assuming an ideal actuator with unlimited velocity and acceleration, they define upper boundaries for the performance of real motors.

The table shows the same influence of the actuator stroke on the step size and the steady state velocity for all investigated modes of operation:

$$\bar{x}_\infty \propto x_{R,\max} \tag{61}$$

$$\bar{v}_\infty \propto x_{R,\max} \tag{62}$$

To achieve high velocities it would therefore be advisable to use ideal actuators with large stroke. In real applications, the actuator bandwidth is a second decisive factor and high bandwidth usually conflicts with high stroke. This topic will be discussed in a future publication.

Figures 10 to 12 show the influence of the rod acceleration factor κ on the three motional performance indicators. For $\kappa \leq 1$ the motor works in stick-slip mode, for $\kappa > 1$ it works in slip-slip mode.

Figure 10 shows that $\bar{v}_\infty$ rises with a_R for modes with continuous slider movement and for discrete stick-slip operation, while it falls with rising a_R in discrete slip-slip operation. The jump in the curve at $\kappa = 1$ results from the sudden change of the slider acceleration at this point if $\mu_0 \neq \mu_d$. The figure

also shows that the maximum velocity reachable in stick-slip operation and/or with discrete steps is limited principally, while continuous slip-slip operation principally allows very high velocities with high κ.

In discrete mode, $\bar{v}_\infty$ is always reached in the first period ($p_{0.99} = 1$), so that the start-up time $T \cdot p_{0.99}$ falls continuously as T falls with rising κ. In continuous stick-slip mode, $p_{0.99} = 2$, so that $T \cdot p_{0.99}$ also falls continuously as T falls with rising κ. In continuous slip-slip mode, $p_{0.99}$ increases with κ, while T decrease with κ. This results in the stair-like line observed in figure 11. Discrete operation generally reaches shorter start-up times.

The smoothness of the slider motion is always 1/2 in discrete mode. In continuous mode, it is always higher than this and rises linearly with increasing κ, as shown in figure 12.

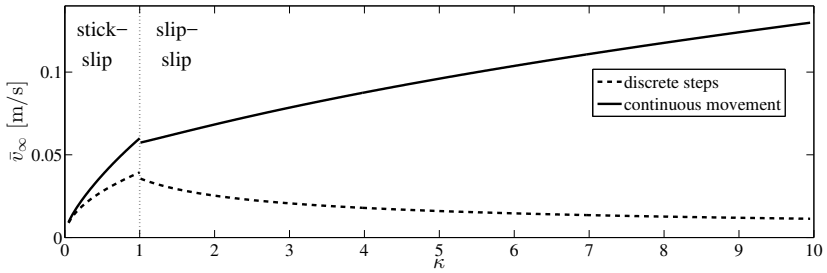

Figure 10: Change of steady state velocity $\bar{v}_\infty$ with changing rod acceleration factor $\kappa = a_R/a_0^+$ for discrete and continuous operation.

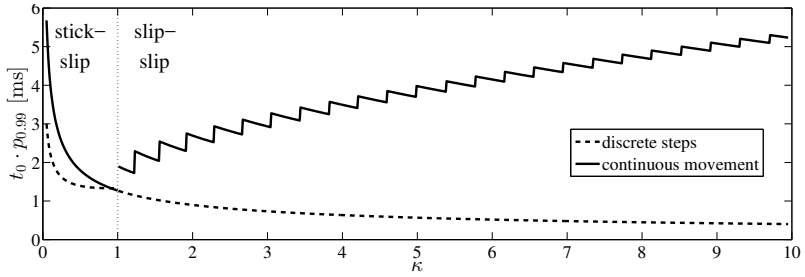

Figure 11: Change of start-up time $T \cdot p_{0.99}$ with changing rod acceleration factor $\kappa = a_R/a_0^+$ for discrete and continuous operation.

4.7. Limitations

The results described in the previous sections have been obtained using some idealisations and assumptions, as described in section 2.2. Their consequences shall be discussed in the following.

The friction contact is modelled using a Coulomb friction model with constant coefficients of static and dynamic friction. Such models are also used by most other authors modelling inertia motors. All works known to the authors

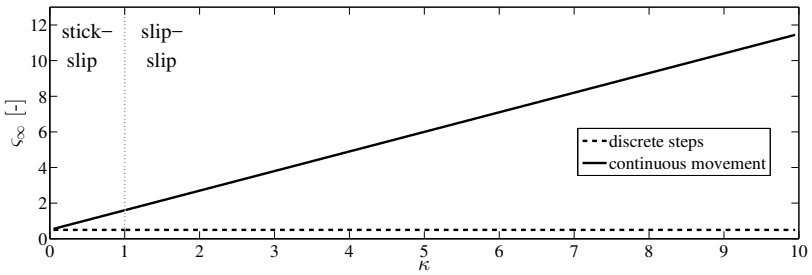

Figure 12: Change of smoothness indicator ς_∞ with changing rod acceleration factor $\kappa = a_R/a_0^+$ for discrete and continuous operation.

that have so far investigated the friction contact in inertia motors in more detail and see the neccessity for more sophisticated friction models concentrate on motors with a step size in the nanometer range [22, 23, 24, 25]. Altpeter [24] has stated that if the actuator stroke is significantly larger then the ratio of the break-away force and the tangential stiffness of the friction contact, kinetic friction models such as the one used in this contribution are accurate enough to model an inertia motor. It is therefore reasonable to assume that for actuator strokes of 25 µm as used in this contribution, the applied friction model is sufficient. With significantly smaller actuator strokes, more sophisticated friction models like the LuGre-model [26] or the elastoplastic friction model [27] can improve the modelling accuracy. But a straightforward derivation of ideal excitation signals as presented in section 4 is not possible with these more complex models. And it is unclear whether these models would lead to significantly different ideal excitation signals.

The investigated motor is driven by an ideal actuator with unlimited bandwidth and acceleration. A real actuator is limited both in bandwidth and in acceleration. For an actuator with limited acceleration but unlimited bandwidth, the excitation signals for maximum velocity are similar to the ones presented in this article, but smoothened around the steep flanks. Such signals are presented and analysed in [20] and [21]. A promising way to obtain drive signals for actuators with limited bandwidth – and consequently also limited acceleration – is to derive them from signals for ideal actuators for example by approximating them using Fourier series. This approach has been successfully investigated by the authors, the results will be presented in the second part of this contribution.

The driving rod is assumed to be a rigid body. As written in section 2.2, this assumption is valid as long as the highest excitation frequency is much smaller than the first eigenfrequency of the rod. This is never the case with the ideal excitation signals, as they contain infinitely high frequencies. Thus the eigenfrequencies of the setup can be regarded as an additional constraint limiting the allowed frequency range when obtaining excitation signals suitable for real motors. If it is not avoided by an appropriate exciation signal, the elastic vibration of the rod can be both longitudinal (x-direction) and perpendicular.

In both cases, these vibrations will lead to a dependence of the slider velocity on its position along the rod. Whether this position dependence is acceptable depends on the application. Another option is to deliberately use resonance effects to obtain large rod displacements at high frequencies [9, 10, 11, 12] or specific vibration modes [13]. In this case, the slider can only move properly on a certain portion of the stator rod depending on the vibration mode. As more than one eigenfrequency has to be excited to obtain the asymmetrical vibration required for inertia motors, the geometry of such a system has to be carefully designed and a proper driving signal has to be used. Such signals will also be discussed in the second part of this contribution.

5. Conclusions

Using the example of a translational inertia motor excited by an ideal displacement signal, it was found that there are four different modes of operation of inertia motors which are differentiated by two criteria:

- Does the slider move in discrete steps or continuously? (discrete or continuous mode of operation)
- Is the propulsion of the slider achieved using stiction or by sliding friction only? (stick-slip or slip-slip operation)

The maximum motor performance achievable in these modes was investigated. One major result is that the maximum velocity reachable in stick-slip operation and/or with discrete steps is limited principally, while continuous slip-slip operation allows very high velocities. It was also found that, for the investigated driving signals whose frequency is proportional to the inverse of the square root of the actuator stroke, the motor velocity is proportional to the square root of the actuator stroke.

The presented results show a clear advantage of slip-slip operation for the design of high velocity inertia motors. This theoretical result is supported by the fact that almost all such motors, reaching high velocities up to $300\,\mathrm{mm\,s^{-1}}$ and published mainly in the last few years [16, 6, 10, 13, 11, 12, 28], are not using stiction but sliding friction for propulsion, even if not explicitly stated in the publications. In the second part of this contribution, the performance of inertia motors driven with frequency-limited signals derived from the ideal signals will be investigated.

Vitae

Matthias Hunstig studied mechanical engineering at the University of Paderborn and graduated with distinction at the end of 2007. Since then he is a research assistant at the chair for mechatronics and dynamics at the University of Paderborn. He started working on different piezoelectric systems as a student, developing energy harvesters and active vibration damping systems. His current main research interests are piezoelectric drives and energy harvesting.

Tobias Hemsel studied mechanical engineering at the University of Paderborn. After graduating in 1996 he was a research assitant at the Heinz Nixdorf Institute of the University of Paderborn and received his PhD in 2001. Since then he is engineering head at the chair for mechatronics and dynamics at the University of Paderborn. His research interests focus on sensors and actuators, especially piezoelectric systems.

Walter Sextro studied mechanical engineering at the University of Hanover and Imperial College in London. After graduating, he designed and optimized drill strings for Baker Hughes Inteq research in Celle, Germany and Houston, Texas. He received his PhD from the University of Hanover in 1997. Subsequently, he qualified as a professor in the field of mechanics and published his habilitation thesis. In 2004 he was appointed as a professor at the institute of mechanics and gear trains at the Technical University of Graz, Austria. Since 2009 he leads the chair for mechatronics and dynamics at the University of Paderborn.

[1] M. Anders, M. Thaer, C. Heiden, Simple micropositioning devices for STM, Surface Science 181 (1987) 176–182.

[2] T. Higuchi, Y. Hojjat, M. Wanatabe, Micro actuators using recoil of an ejected mass, in: Proceedings of the IEEE Micro Robots and Teleoperators Workshop, IEEE, Hyannis, Massachusetts, 1987.

[3] D. W. Pohl, Dynamic piezoelectric translation devices, Review of Scientific Instruments 58 (1987) 54–57.

[4] K. Matsusaka, S. Ozawa, R. Yoshida, T. Yuasa, Y. Souma, Ultracompact optical zoom lens for mobile phone, in: Proceedings of SPIE-IS&T Electronic Imaging, volume 6502, p. 650203 (10 pp.).

[5] K. Uchino, Piezoelectric motors for camera modules, in: ACTUATOR 2008 Conference Proceedings, Bremen, pp. 157–160.

[6] D. Paik, K. Yoo, C. Kang, B. Cho, S. Nam, S. Yoon, Multilayer piezoelectric linear ultrasonic motor for camera module, Journal of Electroceramics 22 (2009) 346–351.

[7] D. A. Henderson, US patent 8059346: Linear drive systems and methods thereof, 2011.

[8] J. Lee, W. S. Kwon, K. Kim, S. Kim, A novel smooth impact drive mechanism actuation method with dual-slider for a compact zoom lens system, Review of Scientific Instruments 82 (2011) 085105.

[9] R. Bansevicius, V. Blechertas, Multi-degree-of-freedom ultrasonic motors for mass-consumer devices, Journal of Electroceramics 20 (2008) 221–224.

[10] B. Koc, Piezoelectric motor, operates by exciting multiple harmonics of a square plate, in: ACTUATOR 2010 Conference Proceedings, Bremen, pp. 194–197.

[11] T. Nishimura, H. Hosaka, T. Morita, Resonant-type smooth impact drive mechanism (SIDM) actuator using a bolt-clamped langevin transducer, Ultrasonics 52 (2012) 75–80.

[12] T. Morita, H. Murakami, T. Yokose, H. Hosaka, A miniaturized resonant-type smooth impact drive mechanism actuator, Sensors and Actuators A: Physical 178 (2012) 188–192.

[13] S. Tuncdemir, S. O. Ural, B. Koc, K. Uchino, Design of translation rotary ultrasonic motor with slanted piezoelectric ceramics, Japanese Journal of Applied Physics 50 (2011) 027301.

[14] C. Edeler, S. Fatikow, Open loop force control of Piezo-Actuated Stick-Slip drives, International Journal of Intelligent Mechatronics and Robotics 1 (2011) 1–19.

[15] C. Edeler, Modellierung und Validierung der Krafterzeugung mit Stick-Slip-Antrieben für nanorobotische Anwendungen, Dissertation, Carl von Ossietzky Universität Oldenburg, 2011.

[16] Y. Okamoto, R. Yoshida, Development of linear actuators using piezoelectric elements, Electronics and Communications in Japan, Part 3 81 (1998) 11–17. Translated from Denshi Joho Tsushin Gakkai Ronbushi, Vol J80-A, No. 10, October 1997, pp. 1751–1756.

[17] M. Hunstig, T. Hemsel, Parameter identification and model validation for the piezoelectric actuator in an inertia motor, Journal of the Korean Physical Society 57 (2010) 952–954.

[18] M. Hunstig, T. Hemsel, W. Sextro, Improving the performance of piezoelectric inertia motors, in: ACTUATOR 2010 Conference Proceedings, Bremen, pp. 657–661.

[19] R. Yoshida, O. Yasuhiro, T. Higuchi, A. Hamamatsu, Development of smooth impact drive Mechanism(SIDM): proposal of driving mechanism and basic performance, Journal of the Japan Society for Precision Engineering 65 (1999) 111–115. (in Japanese).

[20] M. Hunstig, T. Hemsel, Drive signals for maximizing the velocity of piezoelectric inertia motors, Journal of the Korean Physical Society 57 (2010) 938–941.

[21] M. Hunstig, T. Hemsel, W. Sextro, Anregungskonzepte und Modellierung piezoelektrischer Trägheitsmotoren, in: Entwurf mechatronischer Systeme, volume 272, HNI-Verlagsschriftenreihe, Paderborn, 2010, pp. 129–141.

[22] H. van der Wulp, Piezo-driven stages for nanopositioning with extreme stability: theoretical aspects and practical design considerations, Ph.D. thesis, TU Delft, 1997.

[23] J. Breguet, Actionneurs "Stick and Slip" pour Micro-Manipulateurs, Ph.D. thesis, EPFL, Lausanne, 1998.

[24] F. Altpeter, Friction Modeling, Identification and Compensation, Ph.D. thesis, EPFL, Lausanne, 1999.

[25] C. Edeler, I. Meyer, S. Fatikow, Modeling of stick-slip micro-drives, Journal of Micro-Nano Mechatronics (2011) 1–23.

[26] C. Canudas de Wit, H. Olsson, K. Astrom, P. Lischinsky, A new model for control of systems with friction, IEEE Transactions on Automatic Control 40 (1995) 419–425.

[27] P. Dupont, V. Hayward, B. Armstrong, F. Altpeter, Single state elasto-plastic friction models, IEEE Transactions on Automatic Control 47 (2002) 787–792.

[28] M. Suzuki, H. Hosaka, T. Morita, Resonant-type smooth impact drive mechanism actuator with two langevin transducers, Advanced Robotics 26 (2012) 277–290.